Earth Sciences
2022; 11(5): 277-288
http://www.sciencepublishinggroup.com/j/earth
doi: 10.11648/j.earth.20221105.15
ISSN: 2328-5974 (Print); ISSN: 2328-5982 (Online)

The Sliding Surface Investigation of in the West of Koyulhisar (Sivas, Turkey)

Sevda Ozel[1, *], Demet Over[1], Kemal Ozgur Hastaoglu[2]

[1]Department of Geophysical Engineering, Sivas Cumhuriyet University, Sivas, Turkey
[2]Department of Geomatics Engineering, Sivas Cumhuriyet University, Sivas, Turkey

Email address:

sozel@cumhuriyet.edu.tr (Sevda Ozel), demetover@gmail.com (Demet Over), khastaoglu@cumhuriyet.edu.tr (Kemal Ozgur Hastaoglu)
[*]Corresponding author

To cite this article:

Sevda Ozel, Demet Over, Kemal Ozgur Hastaoglu. The Sliding Surface Investigation of in the West of Koyulhisar (Sivas, Turkey). *Earth Sciences*. Vol. 11, No. 5, 2022, pp. 277-288. doi: 10.11648/j.earth.20221105.15

Received: August 23, 2022; **Accepted**: September 21, 2022; **Published**: September 28, 2022

Abstract: The study area covers approximately 200x250 m^2. This area is one of the most active locations with the greatest landslide displacement amount. This study aims to determine the depth of the sliding surface with geophysical (seismic refraction tomography (SRT) and ground-penetrating radar (GPR)) methods. The results of the TUBITAK-111Y111 project were also used in this study. According to the geophysical results, three layers with average seismic P-wave velocities (V_P) of 600, 1200, and 2100 m/sec were identified within an investigation depth of approximately 20 m. It was determined that the depths of the sliding surface changed between approximately 3 to 7 m and seismic velocities were lower than 600 m/sec from these depths to the surface. The geophysical results demonstrated that the landslide type was planar sliding, the sliding direction was S-SE, and the tilt of the geological layer was in the same direction with the topographic slope, mostly bigger than 5^0. It was observed that deformations in the landslide mass were caused by the geological unit, the layer or topographic slope, and precipitation. According to these results the landslide activity may continue in the landslide area and in the study area in the future. Therefore, as a result, it was also expressed that the study area contains the risks and the natural/anthropogenic hazards because the findings show that the settlement area and urban constructions are under threat in the west of Koyulhisar town center.

Keywords: Geophysics-Geodesy, Koyulhisar, Sliding Surface, Landslide, Risk, Hazard

1. Introduction

The landslide is a mass movement and can occur in different forms. The Koyulhisar landslide region is one of the largest active landslide areas, leading to significant loss of lives and property in Turkey. The three most destructive landslides occurred in Koyulhisar (Sivas) on 19 August 1998, 20 July 2000, and 17 March 2005. The Koyulhisar landslides typically occur in the form of debris or mudflow [1, 2]. There has been an increase in landslide activity in Koyulhisar over the past 17 years [3]. The large and small landslides in the Koyulhisar landslide area have mostly occurred due to natural causes until the present day. Artificial causes mainly occur due to human interventions (blasting, drilling, improper planting, loading, loss of vegetation cover, etc.). The last large landslide occurred with the flow of mud in the north of the Koyulhisar landslide area in March 2005. It was determined that this landslide was in the excessively fast (6 m/sec) class in a study [2]. For the landslide in 2000, it was revealed an average slip rate of 2.5-7.4 mm/year [4]. Researchers have stated that landslides usually have a mechanism involving circular rotation; the old landslide mass maintains its activity, and partial landslides occur on the groundmass [2, 5].

The triggering mechanisms of landslides are often complex, and further understanding is required to facilitate the prediction of mobilizations and adequate stabilization and remediation measures. Therefore, it is important to investigate reasons that affect the formation mechanisms and the formation of landslides. Different engineering (geology, geodesy, etc.) disciplines play a significant role in decreasing

landslide effects. They can help to prevent damage by prediction and early warning. In this context, the Koyulhisar landslide area was examined in a wide area with detailed global navigation satellite system (GNSS) methods [6-10] and studies of other disciplines (geology, geochemistry, seismology, meteorology, remote sensing) [1, 4, 5, 11-18]. These studies have identified the annual sliding velocity, sliding direction, displacement amounts, and natural disaster risk of the landslide. It has been determined that the displacement amounts of the landslide velocity vary between 1-8.6 cm/year by topography and geological bedding and that the landslide direction is usually S-SE oriented. At the interpretation stage, the geophysical findings of this study were correlated to the results of all the studies mentioned above. In particular, geophysical tomography (e.g., seismic refraction tomography (SRT), ground-penetrating radar (GPR)) applications are preferred in landslide studies. However, geophysical studies were carried out in a limited area in the project. The structural geometry of the landslide area was delineated with the results of the collected geophysical data. These are seismic V_P velocities, thickness, tilt and direction of layers. Thus, other features such as the sliding surface depth of the landslide, landslide type, advancement direction, and the risk situation were also revealed, and geophysical and other study results were shown to be compatible with each other. The studies by [19-26] are important in this regard. It was carried out multi-methodical geophysical studies containing electrical resistivity, GPR, and seismic methods [27]. It was also carried out similar studies on landslide investigation [28, 29]. In these studies, the sliding surface of the landslides and the flow direction properties of the landslide material were generally determined by 2D (two-dimensional) and 3D (three-dimensional) geophysical sections.

The parameters which define the landslide, such as landslide geometries and bedrock depth or sliding surface depth, have also been determined with SRT and GPR methods in recent years [24-26, 29-31]. Regarding the GPR method, significant studies have been carried out by [32] to reveal soil stratigraphy, by [33, 34] to map faults, fractures and cracks, and by [35-38] to determine groundwater levels. In addition to these, the seismological history, morphological and topographical features, and meteorological data of the study area are always taken into account in the landslide analysis. These data are used to contribute to the interpretations of these studies. Thus, through multi-discipline studies, the landslide type can be determined most accurately by identifying different sliding behaviors (such as the velocity and direction of the landslide, annual amount of displacement) varying from region to region. Landslides that usually occur in the form of sliding may occur with the falling, sliding, and flowing movements or with the combination of a few of these. Therefore, it is very important to accurately determine the landslide type and select methods used in the study. It may be possible to perform an accurate landslide analysis only if these requirements are met. In this article, the above-mentioned issues were examined and discussed separately and together with geophysical results.

2. The Study Area and Surveys

2.1. Seismology

The study area is located in the west of Koyulhisar town center and in the north of the NAFZ (The North Anatolian Fault Zone) (Figure 1). Geological studies demonstrate that the Plio-Quaternary-aged Koyulhisar formation is the youngest unit in the region. It was stated that the youngest unit consisted of talus (slope or deposit) and fluvial conglomerates along the strike-slip faults, and the Koyulhisar section of the NAFZ is still active and a right-lateral strike-slip fault zone due to morphotectonic structures and seismic activities in the region [4, 11, 46]. There are also many old and new landslides in the study area due to the high tilted topography. For these reasons, the directions of movement of the landslides generally threaten the settlement areas [5]. In the study area, it was generally observed that the upper unit was silty sandy clay and sand interbedded silty clay in some places up to about 10 m, and advanced as sand interbedded silty clay and sand interbedded clay in some places toward depths more than 10 m [8, 39]. There is usually the second unit in the east of the study area as the geological unit, and the content of this unit does not change along with depth. Therefore, the second geological unit was considered while interpreting geophysical cross-sections.

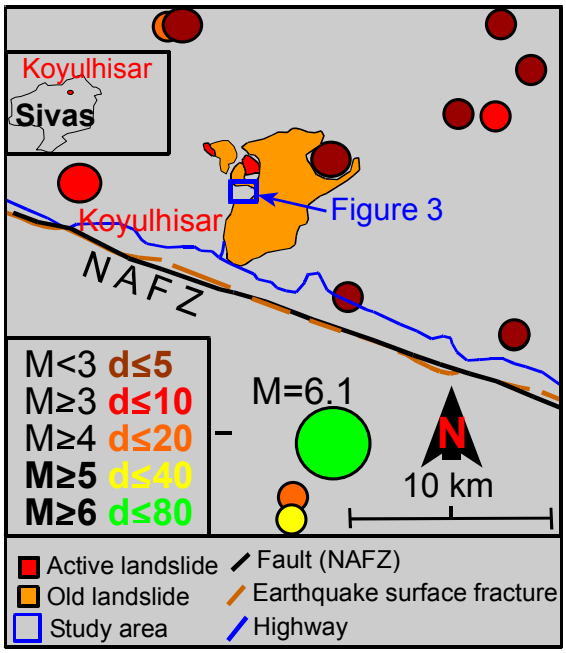

Figure 1. *Seismic activity of the study area and its surroundings by the data between 1900-2015 years and the landslide areas (prepared for this article by integrating from [40, 41].*

The study area is located in an active area in terms of seismicity (Figure 1). The seismological history of the examined area and its surroundings with a magnitude (M) greater than 2.5 was investigated in this article. The seismological data were processed and selected from 1900 to

2015 years (Figure 1) [40]. The type of magnitude calculated from seismological data is usually the local magnitude (M_L). The depths (d) of these earthquakes with M>2.5 vary between approximately 5 and 80 km (Figure 1). According to the seismic data for the years examined, Koyulhisar and its surroundings have always been seismically active. It was observed that the frequency of earthquakes usually occurred on the NAFZ in the south of the study area. Particular attention was paid to the earthquakes before 2005 in the seismological interpretation because the largest and most recent landslide occurred in the area in 2005, and it was aimed to investigate its relationship with displacements and previous landslides. It was analyzed the seismic activity of the region (1904-2016) [18] and stated that the relationships between the magnitude of the earthquake and the number of landslides and between the magnitude and the maximum distance of landslide observations from the epicenter under different geological, topographical, and climatic conditions were probably the most remarkable. Large earthquakes affecting the Koyulhisar district also occurred in the region. These earthquakes were in the south of the NAFZ or Suşehri district, and three large earthquakes with M≥5.6 occurred there [3]. The 1992 earthquake is closest to the study area with the least depth but is the second largest earthquake (Figure 1). This earthquake is an earthquake with a 6.1 magnitude that occurred 10 km below the ground. The large earthquakes in the south of Suşehri district, which is just 13 km away from the study area, also occurred in 1909 and 1939. The 1909 earthquake occurred 60 km below the ground and is the largest and deepest earthquake with a magnitude of 6.3. The 1939 earthquake is also deep and the third largest earthquake that occurred 50 km below the ground with a magnitude of 5.6 [3]. It was observed that the magnitudes of the other earthquakes in the north of the NAFZ and the upper elevations of the landslide generally vary between 2.5-4 (Figure 1). Likewise, the other earthquakes in the south of the landslide area are earthquakes with a magnitude greater than 3.6. All these earthquakes may have triggered the landslide mass from time to time in places where sliding surfaces, layers, and topography in the landslide area are inclined more than 5-10 degrees (according to the geophysical cross-sections in this article, when it is considered that there are loose units and deformations on the sliding surfaces). In particular, they further affected the landslide mass along with the rainfall and caused large amounts of displacement in the landslide area.

2.2. The Interpretation of Meteorological and Geodetical Results

The data on the rainfall triggering landslides are presented in this section (Table 1, Figures 2a-b). With these data, the rainfall status of the study area and its surroundings was examined by months as average annual rainfall and the annual areal amount of rainfall. According to the data obtained between 1950-2015 (Table 1), rainy periods are generally between October-November-December and January-February-March-April. The highest total daily amount of rainfall in the rainiest years was observed as snowfall in 1950 (110 cm) and as rainfall in 1991 (55 kg/m^2). The annual normal average rainfall value for the years 1981-2010 was calculated as over 483.4 mm (Figure 2a) [42]. However, 1987-1988 and 1997-1998 were the rainiest years. It is seen that the annual areal amount of rainfall exceeded the normal values and was higher than 550 mm in these rainy years that took place every 10 years. Likewise, there were high rainfalls for 3-4 years after 1985-1995-2005 with an interval of 10 years. Therefore, annual areal rainfalls were observed more before some large landslides like the landslide in 1998. When geological features of the region are taken into account, it is remarkable that the landslides in 1998 and 2000 occurred in the summer months after a winter season with heavy snow. However, the landslide in 2005 occurred during the rainy season.

Table 1. *The annual average meteorological values at between 1950-2015 years, in Sivas [42].*

Sivas	**Jan Feb Mar Apr May Jun Jul Aug Sep Oct Nov Dec**
The average tempreture (°C)	-3.2 -2.0 2.9 9.1 13.5 17.2 20.2 20.2 16.2 10.8 4.6 -0.6
The average the highest tempreture (°C)	1.0 2.6 8.1 15.3 20.0 24.0 27.9 28.5 24.7 18.4 10.6 3.7
The average the lowest tempreture (°C)	-7.0 -6.2 -1.7 3.4 7.2 9.9 12.0 11.9 8.3 4.4 -0.2 -4.2
The average sunshine duration (hour)	2.3 3.3 4.5 6.2 8.1 10.4 12.1 11.4 9.4 6.3 4.1 2.3
The average number of rainy days	13.0 12.4 13.7 14.0 14.4 8.8 2.5 2.1 4.3 8.0 9.5 12.1
The average monthly total rainfall (kg/m^2)	42.0 40.3 46.0 59.1 60.7 34.8 8.5 5.9 16.9 32.9 41.0 44.2
The highest and the lowest values occurring over many years (1950-2015)	
The highest tempreture (°C)	14.6 18.1 25.2 29.0 32.0 35.5 40.0 39.4 35.7 30.5 22.8 19.4
The lowest tempreture (°C)	-34.6 -34.4 -27.6 -10.9 -4.2 -0.3 3.4 3.2 -3.8 -8.1 -24.4 -27.0
Daily total the highest rainfall 2 May 1991: 55.0 kg/m^2	
Daily the fastest wind 5 Jan. 1996: 122.8 km/h	
The highest snow 2 Feb. 1950: 110.0 cm	

GNSS and multi-disciplinary studies by [8] were carried out for long years (about 6 years) to determine the deformation and annual sliding amounts, especially after the landslides in 1998-2000-2005 (Figure 2b). The seismological and meteorological data, updated by the geodetic (GNSS (DH), geological (IDH (Inclinometer Drilling Holes)) and meteorological data collected in this local study, were reorganized and evaluated. Which were prepared for the study area (Figure 2a, Table 1), the subject of this article, were associated with the results of GNSS studies (Figure 2b). The monthly and annual meteorological data should be evaluated within the scope of monitoring activities since the area is a landslide area. It was carried out monitoring in DH wells in the area in 2013-2014 (Figure 2b) [8]. There are seven DH

points in the nearest of the geophysical profiles (DH8, DH12, DH16 are near area A, and DH4, DH6, DH9, DH10 are near area C). (Figure 3a). The graphics (Figure 2b) was prepared from the combined data (unpublished data in the project), and the temperature (°C), precipitation (m^3), and soil moisture content (cm) were compared in these graphics. The temperature and precipitation were inversely proportional during the summer months, called a dry period. It is seen that the soil moisture is changeable apart from the rainy period and has a very high water content during the rainy periods. The soil moisture is very high (average 150 cm) in the winter, summer, and autumn seasons. In the study area, the water contents in the drilling data change from 24.6 % to 13.3 % at a depth between 0-10 m, and these values are also high (from 29.1% to 17.3%) after 10 m. The water generated by precipitation and melting snow is blocked by the impermeable layer when it infiltrates downward, and the local moisture content increases [24]. Thus, the water infiltrates the interface between the permeable and impermeable layers and can form a slip zone. Then, these results were compared with geophysical results in interpretation. The GPR results show that the moisture content of soils on the sliding surface of the landslide mass is relatively high. The drilling data and soil moisture values also show a very high moisture content of the sliding surface of the landslide mass in the study area, which is completely consistent with the results obtained from the GPR-SRT profiles, meteorological and geological results. On the other hand, it was understood that precipitation increased with a decrease in temperatures. It is also seen that the total annual amount of rainfall increased about 2-fold in 2014 compared to 2013 (Figure 2). According to all results, rainfall is considered to trigger landslides because the ground of this landslide area, filled with loose units and old cracks, is supersaturated with water due to rainfalls. Besides, the groundwater level gets close to the surface for 4-6 m on average at the end of the rainy period. However, this level is approximately 10 m at the end of the rainy period and approximately 25 m in some wells in the area where the geophysical study area is also located, and the groundwater flow direction is SW [8]. Consequently, when the displacements and landslide directions estimated from GNSS measurements were also considered, it was determined that these results were compatible with the geophysical sections and the rainfalls were among the reasons triggering landslides.

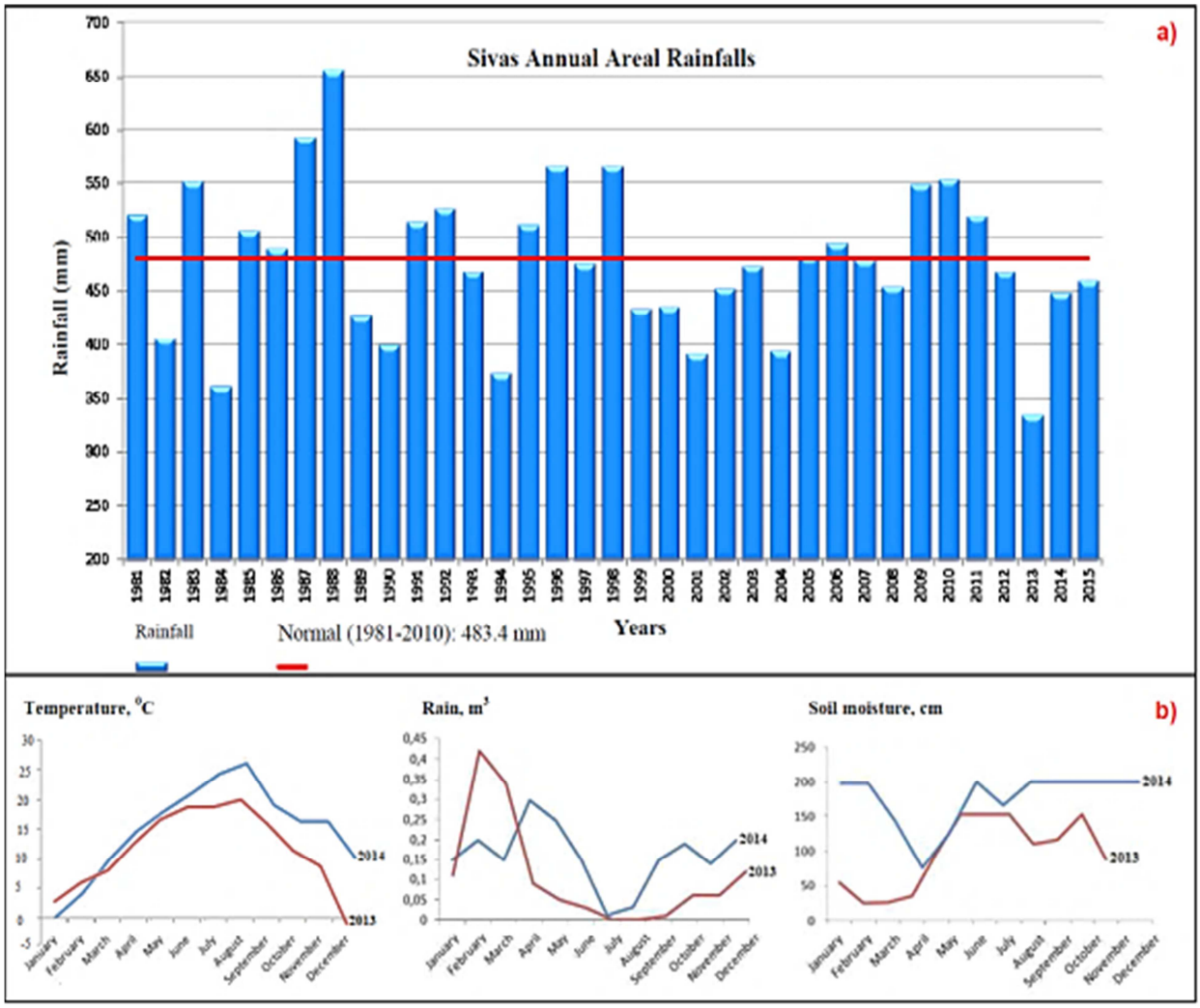

Figure 2. *a Precipitation distribution in between 1981-2015 years of Sivas (prepared from [42]) b Graphics of monthly average temperature (T, °C), rainfall (m^3) and soil moisture content (cm) of the study area and its surroundings in the years of 2013 and 2014 (prepared from the TÜBİTAK-111Y111 project data).*

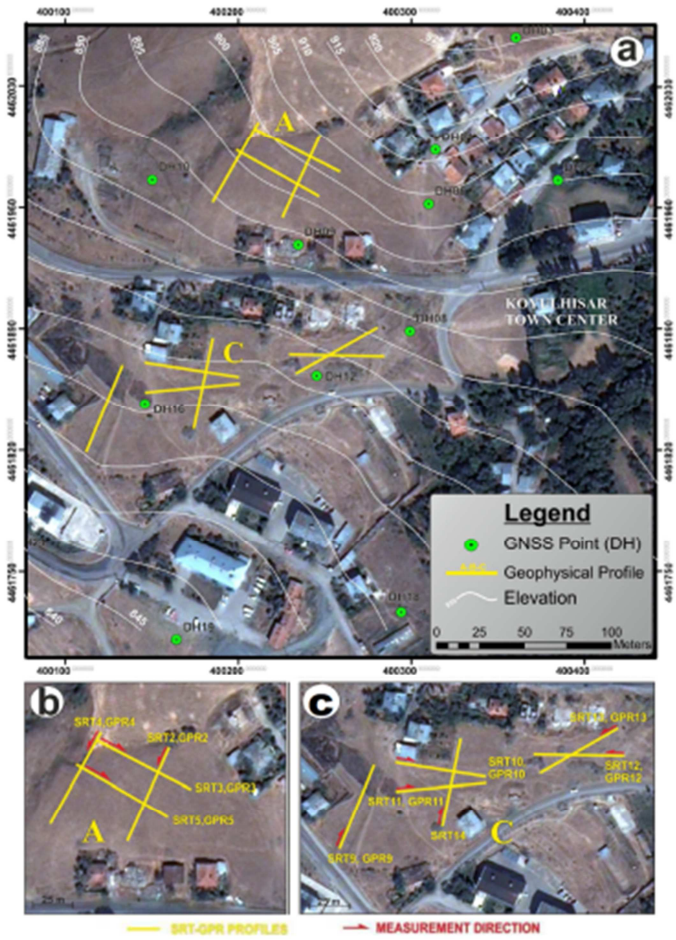

Figure 3. *a The study area. b and c The details of geophysics profiles for the A and C areas).*

2.3. Geophysical Surveys

In this article, geophysical surveys cover a limited area of approximately 200x250 m^2. Seismic refraction tomography (SRT) and ground-penetrating radar (GPR) methods are applied in the tomography format. The SRT method determining seismic P-wave velocities (V_P) for seismic applications and the GPR method for electromagnetic (EM) applications were used in the geophysical data collection in the area (Figure 3). High-frequency electromagnetic waves can penetrate deeper in environments with low conductivity, like sand. However, conductive units, such as clay and shale, decrease the penetration depth of the signal transmitted and lead to absorption [43, 32]. Firstly, SRT and GPR data were collected along multiple transects in two different areas of the study area named A and C (see Figure 3). Then, the geophysical profiles were processed to the satellite map according to the coordinates along with the topographic elevation curves and GNSS measurement locations for ease of interpretation (Figure 3a). Geophysical measurements were taken due to the geologic bedding and topographic features (Figures 3b-c). SRT profiles and GPR profiles on these seismic profiles in the area defined by A in Figure 3b are approximately in the NE-SW (SRT2, SRT4, GPR2, GPR4) and NW-SE (SRT3, SRT5, GPR3, GPR5) directions (Figure 3b). Similarly, in area C, SRT11-SRT12-GPR11-GPR12 profiles are approximately in the E-W direction, SRT9-SRT14-GPR9-GPR14 profiles are approximately in the NE-SW direction, SRT10-GPR10 profiles are in the NW-SE direction, and SRT13-GPR13 profiles are approximately in the NE-SW direction (Figure 3c). The profile lengths usually range from 25 to 60 m, according to the method applied.

The profile shooting technique in the seismic study, a hammer and iron plate with a weight of 8 kg as the source P geophone of 14 Hz (the total number of geophones is 12), and a Geometrics-branded seismic device as the receiver were used while collecting SRT data. In all profiles, the geophone interval was 5 m, the offset distance was 2.5 m, the sampling interval was 256 ms, and the record length was 512 ms. The geophones were respectively fixed on the ground within the selected geophone range, and their connections with the seismic device were established. Then, seismic measurements were recorded by starting from the offset distance of 2.5 m, reducing to a sledgehammer plate and making at least 5 times shots between each geophone, respectively. In the evaluation of the SRT data collected in the field, the SeisImager program was used to display, process, and evaluate seismic refraction waves. The first arrivals of the SRT data were marked using Pickwin, and the evaluation of the first arrival data was performed using the Plotrefa module. The GPR data were collected with a Ramac2 device using a shielded antenna of 250 MHz. The GPR data were processed in the Reflexw program. To collect the GPR data, other parameters were selected as 512 ns-number of samples, 16-number of stacking, and 0.1 m-trace interval. Two-dimensional GPR data processing for data analysis of the GPR data includes static correction (10 ns in dry or wet clay and sand), muting, bandpass filter (100, 200, 300, 400 Hz), gain (0.512 ms), and migration (0.01 ms) steps. The migration was performed to reveal small vertical structures invisible during data processing. Thus, very large hyper balls with strong reflections may limit the display of non-migrated GPR data. Moreover, the peak points of hyperbolas observed in GPR cross-sections show the reflection surface of the electromagnetic wave. During data processing, velocity analysis was conducted on the reflection surfaces through the hyperbola superposition method, and EM wave propagation velocity was calculated in all GPR cross-sections.

The topographic corrections were made by selecting the “Correct for two layers” option in static correction/muting in the Reflex program. The height values collected in the study area were manually entered and saved in the “Correct for two layers” option. Thus, the cross-sections were converted from ns to m, and the GPR sections were prepared for interpretation. Thus, the collected geophysical data were converted into 2D (two-dimensional) elevation-distance (SRT) and depth-distance (GPR) sections by assessing them in the appropriate software. The geophysical study area is one of the most active locations in the landslide area. Geomorphologically, the landslide cracks on the surface,

displacement traces, and structural damages in the study area and its immediate surroundings can be monitored clearly in this activity area (Figure 4). The damaging effects of currently active or old landslides on residences, roads, and walls are also easily observed with field observations. Therefore, none of the damaged constructions are used in Koyulhisar.

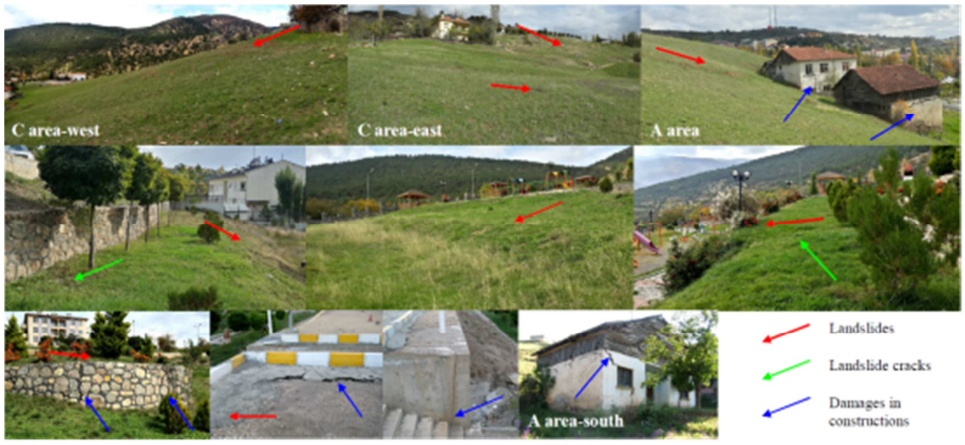

Figure 4. *The photos of the study area and its surroundings, in which the landslides, landslide cracks or constructional damages are also observed.*

3. Results and Discussion

Geophysical interpretations were made according to the geophysical sections and compared with the results of other studies.

3.1. SRT Sections

Two-dimensional seismic cross-sections giving seismic V_P-depth information are presented in Figures 5 and 6. In the seismic data evaluation, coincidence was provided with RMS (Root Mean Square) errors ranging between 3.4-4.5% in 2D inversion operation. According to these sections, two or three layers were identified at a depth of about 20 m (Figures 5-6). It was understood that the tilts of these layers were southeast-oriented, and their tilt was greater than 5^0. According to the average seismic velocities (V_P) calculated, three layers with layer velocities of 600, 1200, and 2100 m/sec were defined from top to bottom. Thus, seismic V_P velocities were observed to increase toward the depth. It was determined that the depth of the sliding surface varied between 3-7 m (Figures 5-6). Therefore, these depths were defined as the layer with the risk of dislocation. This area was considered to have a risk of dislocation due to these loose units, rainfall, and tilt conditions. The seismic velocity of the first layer is lower than V_{P1}<600 m/sec, but the seismic velocity of the third layer may be greater than V_{P3}>2100 m/sec.

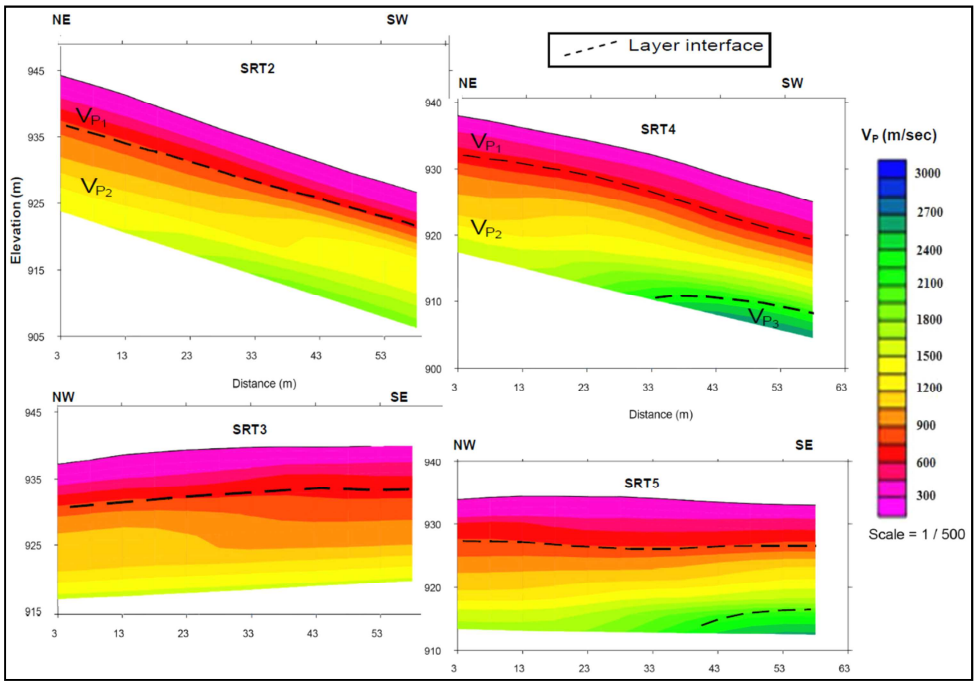

Figure 5. *The seismic profiles of the area A. The uppermost boundary of the V_{P2} layer is the depth of the sliding surface (This depth changes between ~3-7 m). The lower velocity V_{P1} layer consists of soil and alluviums (the average seismic V_{P1}< 600 m/sec).*

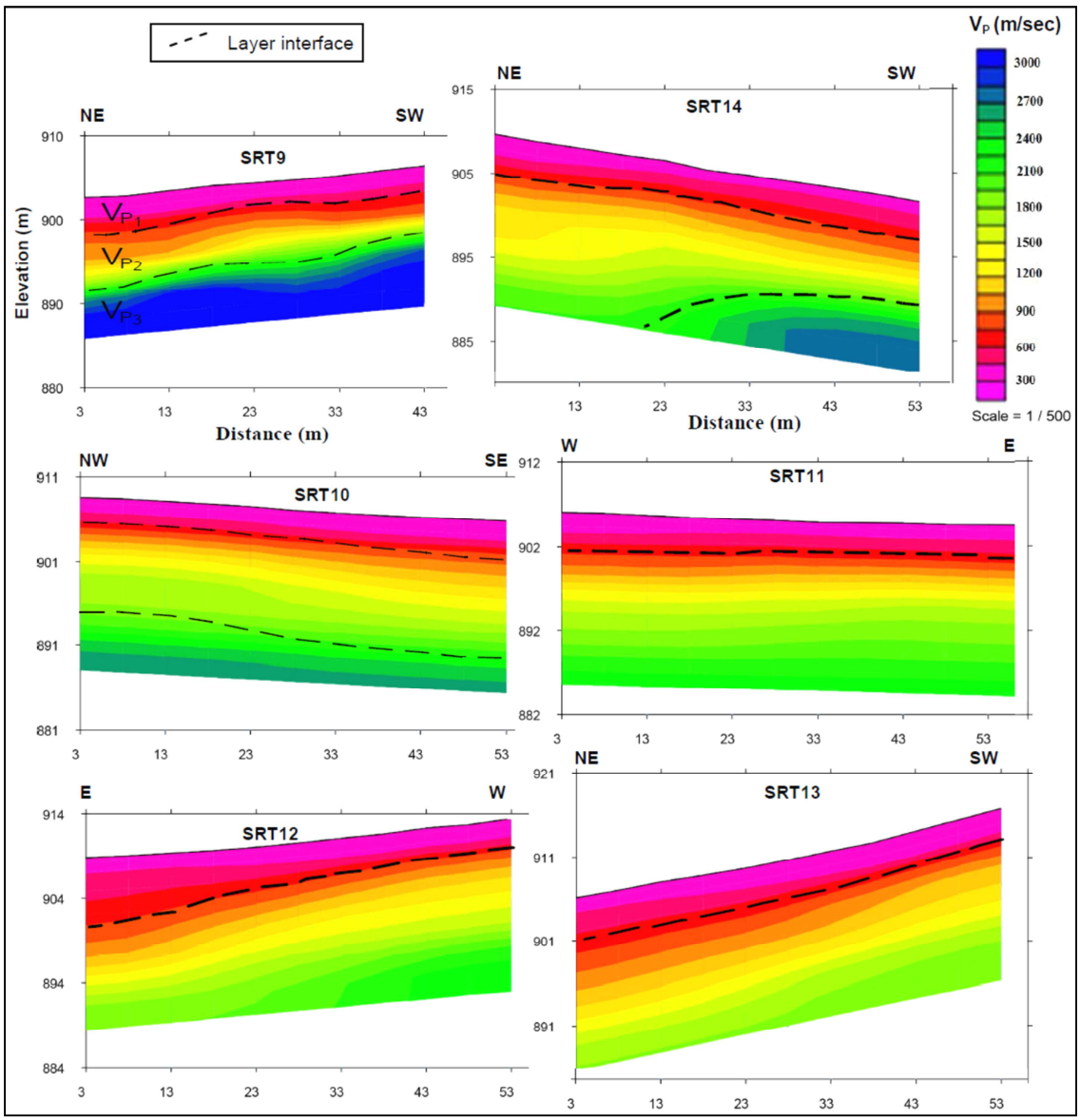

Figure 6. *The seismic profiles of the area C. The uppermost boundary of the V_{P2} layer is the depth of the sliding surface (This depth changes between approximately 3 to 7 m). The lower velocity V_{P1} layer consists of soil and alluviums (the average seismic V_{P1}< 600 m/sec).*

3.2. GPR Sections

The investigation depth was further calculated from the SRT sections compared to the GPR sections due to differences in geophysical methods in the application because the GPR sections were obtained in high resolution for the depth of about the first 10 m after data processing of the GPR data. It is observed that the strong reflections are within the depth of 10 m (Fiures 7-8). These strong reflections seen in black dashed ellipses are interpreted as deformation areas in the layer. Similarly, these areas being interpreted as deformations were also observed in the studies by [24-26, 38]. The strong reflected wave signal displays distinctive characteristics, presenting a low-frequency high-amplitude sync-phase axis, which can be inferred as the sliding surface (Figures 7-9). In other words, two layers were identified in the GPR sections. The first layer is weak, loose, cracked, moved, has lost its tightness, and has low seismic velocity. Therefore, it was thought that deformations developed on the sliding surfaces due to the geology of the study area in areas A and C (Figures 7-9). Deformations, called sliding surfaces, landslide furrows, scarps, collapsed zones, and cracks, were identified. If areas of A and C are compared, more deformations are observed in area C than in area A. Therefore, the risk of landslides may be higher in area C. The EM wave velocity calculated for the reflection surface in the GPR5 cross-section representing the GPR profiles was shown as an example (Figure 7). Picks were exported with the attribute of two-way travel time, and the velocity of propagation of the wave was calculated as about 0.1 m/ns (Figure 7). This value is generally observed in dry or wet soil, dry or wet clay and sandy environments [44, 45]. Therefore, this velocity value was thought to be compatible with the geological units, and electromagnetic waves led to rapid absorption due to the silty

sandy clay layer because the first geological unit is medium-very stiff, silty sandy clay, and has low-high plasticity. Deformation structures, such as sliding surfaces, landslide furrows, scarps, collapsed zones, and cracks, were observed in the GPR cross-sections (Figures 7-9). In other words, the geological unit, the layer or topographic slope, and precipitation cause deformations in the loose upper unit. Therefore, these structures may develop or occur in the landslide mass, as shown in Figures 7-9.

Consequently, the geological units observed in DH wells are mostly silty sandy clay, and they have different characteristics above and below 10 m in DH wells. The topography of the study area decreases from 925 m to 840 m, and the elevation difference is 85 m (Figure 3). The amount of slope in the topography increases from south to north ($>5^0$-10^0) in the geophysical sections (Figures 5-6). It was determined that the landslide type in the area was planar sliding and the direction of sliding was SE. Since this information was associated with topography and field observations, it was observed that the topography was inclined from the north to the south of the study area. The results of various studies and the findings of this article have proved that Koyulhisar landslides are generally caused by the known reasons that trigger landslides. Therefore, it was revealed that the geological bedding was compatible with the topographical sloping and the groundwater was compatible with the flow direction.

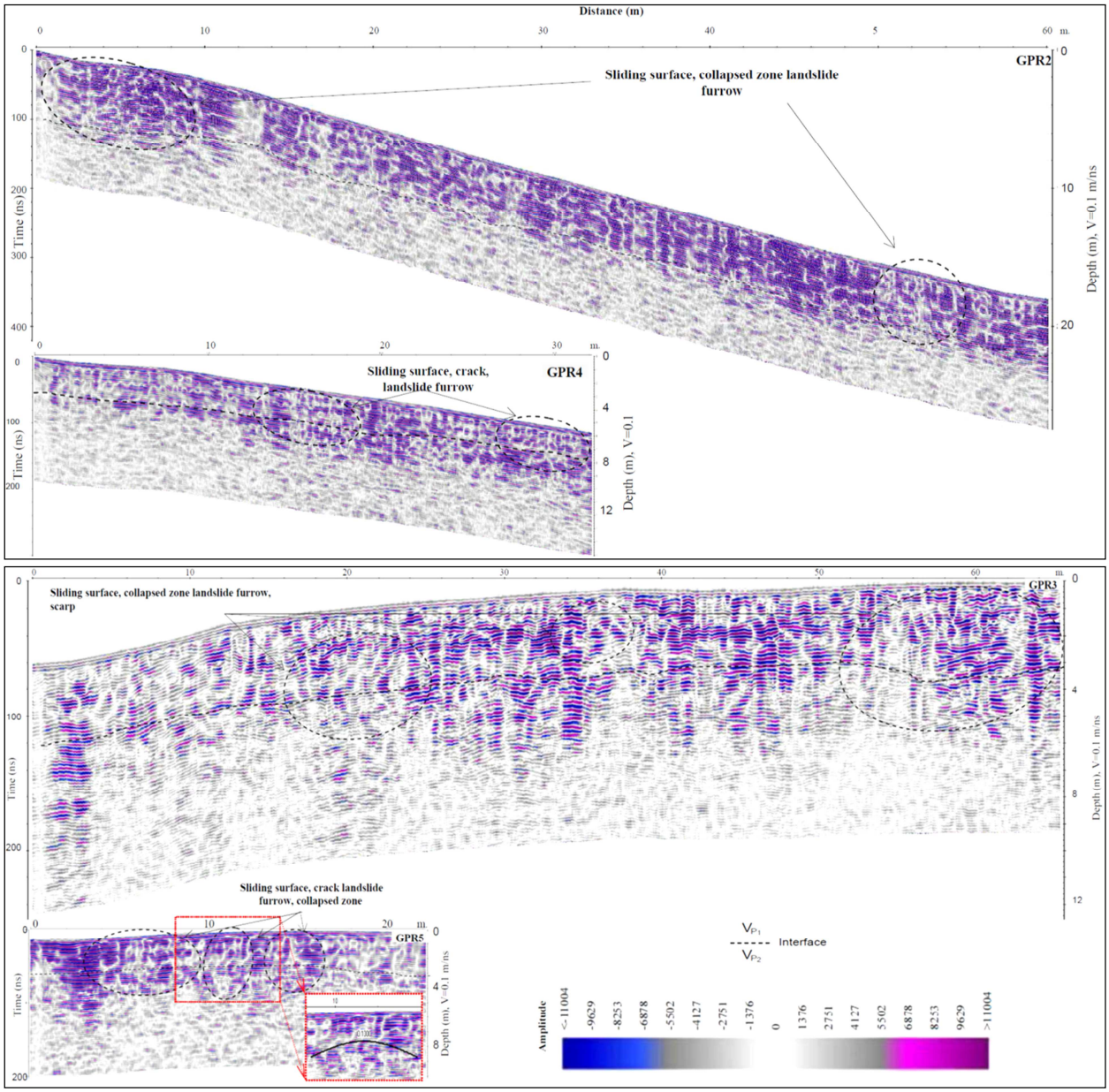

Figure 7. *GPR profiles in A area and the deformations in the loose layers (the seismic V_{P1} layer=the sliding mass).*

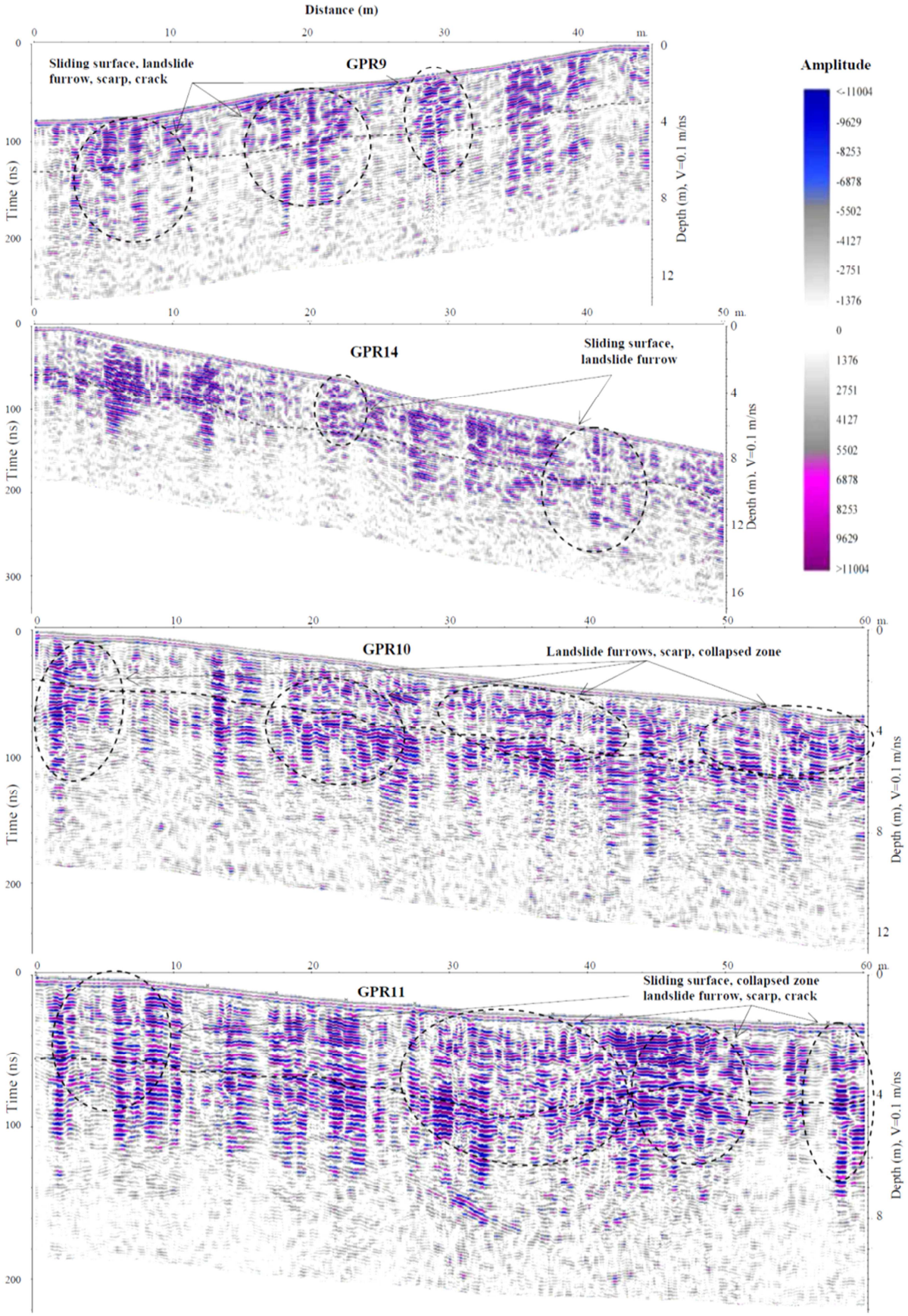

Figure 8. *GPR profiles in the C-west area and the deformations in the loose layer (the seismic V_{P1} layer=the sliding mass).*

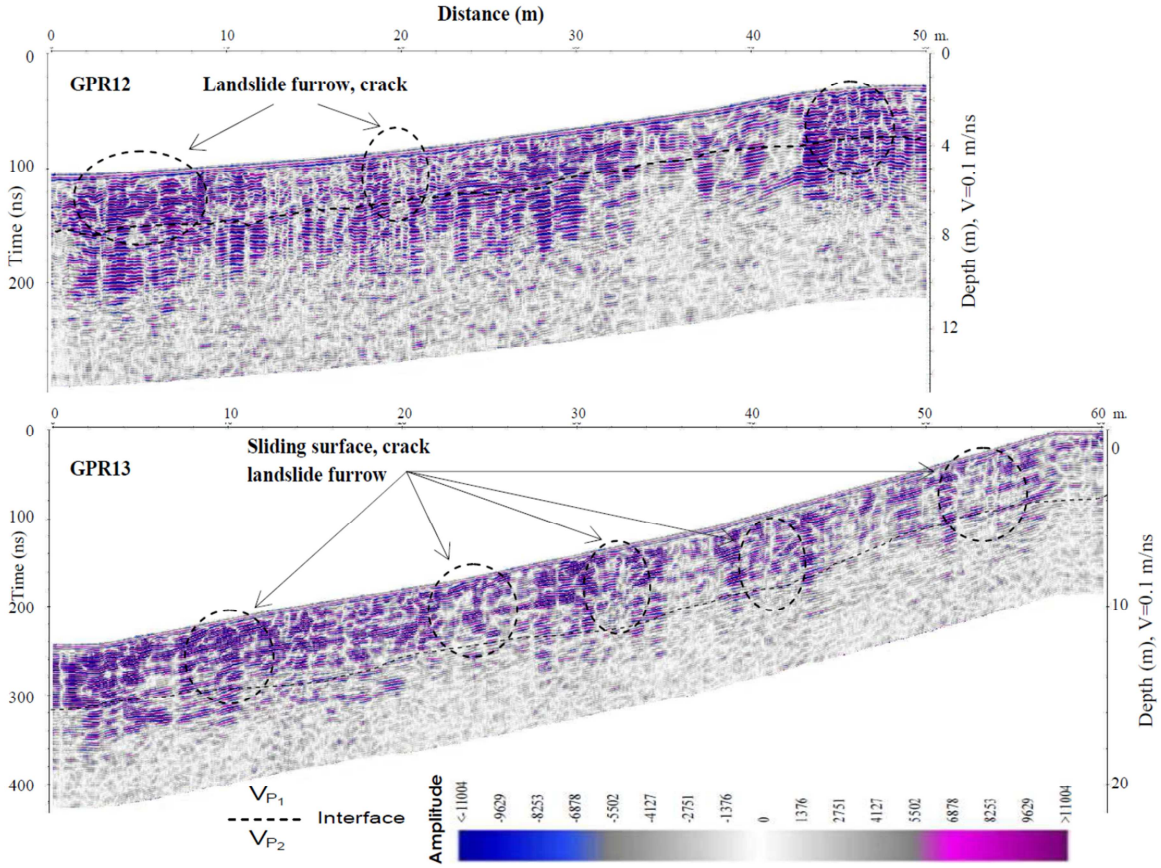

Figure 9. *GPR profiles in the C-east area deformations.*

If the square-shaped pixel size in our images was 8 × 8 screen-pixels, this amounted to about 21 pixels per face quantization (an equivalent of about 10.5 cycles/face). With this level of image detail, all three basic varieties of configural information (hange of spatial quantization between 11 pixels/face and 6 pixels/face levels altogether indicate that this ERP- component is especially sensitive to the first-order configural cues. Some other works have supported both of these ideas.

4. Conclusion

Landslides may develop under various geological, morphological, topographical, and physical conditions. The information provided from many studies (geodetic, geological, morphological, seismological, topographic, and meteorological) carried out across the region was compared with geophysical results (SRT and GPR) and found compatible. The seismic P-wave velocity (V_P) of the layers, the tilt, tilt direction of the layers, depth of the sliding surface, sliding direction, and the landslide type were determined from the geophysical sections. The study area was identified by the three layers. It was revealed that the depth of the sliding surface varied between 3-7 m due to topographical differences in the geophysical cross-sections. These depths were the depths with low seismic velocities (<600 m/sec) and were defined as loose units, which were also observed in geological drilling logs. Sliding surfaces, landslide furrows, collapsed zones, scarps, and cracks were observed in the landslide mass in the GPR sections. It was observed that the layer tilt was generally more than 5^0 in all geophysical sections and compatible with the geology and flow direction of the groundwater. The landslide type in the area was planar sliding, and the sliding direction was SE. The geophysical and other results were found to be compatible because it is known that the landslide direction across Koyulhisar is S-SW and SE. Consequently, the fact that the depth of the sliding surface over the geologic unit is loose, the seismic velocity of the upper layer is low, and the tilt is excessive shows that there is a risk of a new landslide in the area. Therefore, there is still a high landslide hazard in the study area and its surroundings, and this hazard will also continue in the future. The other factors triggering landslides were found to be associated especially with the fact that the area is seismically active, receives heavy rain and has a poor vegetation cover. On the other hand, it was thought that blasting and excavation performed by humans could trigger landslides due to the geologically loose unit. Hence, the landslide area can be a potential area open to natural/artificial hazards. The identified risks and natural hazards also threaten the settlement area, buildings, and other constructions (roads, walls, parks, buildings) in Koyulhisar.

Acknowledgements

This study was supported by Sivas Cumhuriyet University Scientific Research Projects Commission as CUBAP Project numbered M-464. We would like to thank the Project Coordinator Prof. Dr. Kemal Ozgür Hastaoglu and his research team, who allowed us to benefit from the results of the TUBITAK (The Scientific and Technological Research Council of Turkey) project numbered 111Y111. We would like to thank Dr. Cagri Caylak for his contributions during the geophysical field measurements, Prof. Dr. Fatih Poyraz for his contributions during the geodetic field measurements. We also would like to thank the Geological Engineer Mehmet Demirel for his contributions to Figure 3.

References

[1] Tatar, O., Gürsoy, H., Altunel, E., Akyüz, S., Topal, T, Sezen, T. F., Koçbulut, F., Mesci, L., Kavak, K. Ş., Dikmen, Ü, Türk, T., Poyraz, F., Hastaoğlu, K. Ö., Ayazlı, E., Gürsoy, Ö., Polat, A., Akın, M., Demir, G., Zabcı, C., Karabacak, V., Çakır, Z. (2007). Natural disaster risk analysis of residential areas along the Kelkit Valley on the North Anatolian Fault Zone, GIS-based disaster information system (KABİS) design: project introduction and preliminary findings. the Active Tectonics Research Group (ATAG), 11th Workshop, TUBITAK-MAM Institute of Earth and Marine Sciences Gebze-Kocaeli, Turkey, 14-16, https://atag.itu.edu.tr/dosya/ATAG11bildiriozleri.pdf, http://www.koyulhisar.gov.tr /bulten3.doc, (in Turkish).

[2] Duman, T. Y., Nefeslioğlu, H., Gökçeoğlu, C., & Sönmez, H. (2005). 17/03/2005 Kuzulu (Sivas-Koyulhisar) landslide. General Directorate of Mineral Research and Exploration, Department of Geological Studies, Hacettepe University, https://www.mta.gov.tr/v3.0/sayfalar/bilgi-merkezi/deprem/pdf/sugozu_heyelani.pdf (in Turkish).

[3] Över, D. (2015). The Research of the landslide area ground of Koyulhisar district in Sivas with geophysical methods. Sivas Cumhuriyet University, MS Thesis, Sivas, Turkey.

[4] Demirel, M., Tatar, O., Koçbulut, F. (2016). Kinematics of the faults around the Koyulhisar (Sivas) region on the North Anatolian Fault Zone. Geol. Bull., 59 (3): 357-370 (in Turkish).

[5] Sendir, H., & Yılmaz, I. (2001). Structural and geomorphological perspective on Koyulhisar landslides. Journal of Cumhuriyet University Faculty of Engineering, Series A: Earth Sciences 18 (1): 47-54 (in Turkish).

[6] Hastaoğlu, K. O., & Şanlı, D. U. (2011). Monitoring Koyulhisar landslide using rapid static GPS: a strategy to remove biases from vertical velocities. Nat. Hazards, 58: 1275-1294. DOI: 10.1007/s11069-011-9728-5.

[7] Hastaoğlu, K. O. (2013). Investigation of the groundwater effect on slow-motion landslides by using dynamic Kalman filtering method with GPS: Koyulhisar town center. Turkish J. Earth Sci., 1033-1046. DOI: 10.3906/yer-1210-10.

[8] Hastaoğlu, K. Ö., Türk, T., Koçbulut, F., Balık Şanlı, F., & Poyraz, F. (2015). Monitoring landslides and performing disaster information system-based risk analysis using GNSS and PS-InSAR methods: Koyulhisar (Sivas) landslides. Final report. TUBITAK Project Number: 111Y111, Program Code: 3501, Turkey (unpublished).

[9] Hastaoğlu, K. O. (2016). Comparing the results of PSInSAR and GNSS on slow motion landslides, Koyulhisar, Turkey. Geomatics Nat. Hazards and Risk, 7 (2): 786-803. DOI: 10.1080/19475705.2014.978822.

[10] Hastaoglu, K. O., Poyraz, F., Turk, T., Yılmaz, I., Kocbulut, F., Demirel, M. & Balik Sanli, F. (2018). Investigation of the success of monitoring slow motion landslides using Persistent Scatterer Interferometry and GNSS methods. Survey review, 50 (363), 475-486. DOI: 10.1080/00396265.2017.1295631.

[11] Toprak, G. M. V. (1989). Tectonic and stratigraphic characteristics of the Koyulhisar segment of the North Anatolian Fault Zone (Sivas-Turkey). METU (Middle East Technical University) (unpublished), Ph.D. Thesis, Ankara, Türkiye.

[12] Uysal, S. (1995). Koyulhisar (Sivas) yöresinin jeolojisi. General Directorate of the Mineral Research and Exploration (MTA) Report number: 9838 (in Turkish).

[13] Sendir, H., & Yılmaz, I. (2002). Structural, geomorphological and geomechanical aspects of the Koyulhisar landslides in the North Anatolian Fault Zone (Sivas, Turkey). Environ. Geol., 42: 52-60. https://doi.org/10.1007/s00254-002-0528-9

[14] Yılmaz, I., Ekemen T., Yıldırım, M., Keskin, İ., & Özdemir, G. (2005) Failure and flow development of a collapse induced complex landslide: the 2005 Kuzulu (Koyulhisar, Turkey) landslide hazard. Environ. Geol., 49: 467-476. DOI: 10.1007/s00254-005-0113-0.

[15] Gökçeoğlu, C., Nefeslioğlu, H. A., Sönmez H., Duman, T., & Can, T. (2005b). The 17 March 2005 Kuzulu landslide (Sivas, Turkey) and landslide-susceptibility map of its near vicinity. Eng. Geol., 81 (1): 65-83. DOI: 10.1007/s00254-006-0322-1.

[16] Yılmaz, I. (2009) A case study from Koyulhisar (Sivas-Turkey) for landslide susceptibility mapping by Artificial Neural Networks. Bull. Eng. Geol. and the Environ., 68: 297-306. DOI 10.1007/s10064-009-0185-2.

[17] Topal, T., & Hatiboğlu, O. (2015). Assessment of slope stability and monitoring of a landslide in the Koyulhisar settlement area (Sivas, Turkey). Environ. Earth Sci., 74 (5). DOI 10.1007/s12665-015-4476-6.

[18] Demir, G. (2018). Landslide susceptibility mapping by using statistical analysis in the North Anatolian Fault Zone (NAFZ) on the northern part of Suşehri Town, Turkey. Nat. Hazards, 92: 133-154. https: //doi.org/10.1007/s11069-018-3195-1.

[19] McCann, D. M., & Forster A. (1990). Reconnaissance geophysical methods in landslide investigations. Eng. Geol., 29 (1): 59-78. https://doi.org/10.1016/0013-7952(90)90082-C

[20] Demirağ, O. (1991). Jeofizik yöntemlerle heyelan araştırmaları. TMMOB-JFMO (The Chamber of Geophysical Engineers of Turkish) publications. Jeofizik, 5 (1), 43-50, Ankara, Turkey (in Turkish).

[21] Hack, R. (2000). Geophysics for slope stability. Surv. Geophys., 21: 423-448. https://doi.org/10.1023/A:1006797126800.

[22] Perrone, A., Iannuzzi, A., Lapenna, V., Lorenzo, P., Piscitelli, S., Rizzo, E., & Sdao, F. (2004). High-resolution electrical imaging of the Varco d'Izzo earthflow (southern Italy). J. Appl. Geophys., 56: 17-29. DOI: 10.1016/j.jappgeo.2004.03.004.

[23] Göktürkler, G., Baklaya, Ç., & Erhan, Z. (2008). Geophysical investigation of the landslide: The Altındağ landslide site, Izmir (western Turkey). J. Appl. Geophys., 65: 84-96. https://doi.org/10.1016/j.jappgeo.2008.05.008

[24] Hu, Z., & Shan, W. (2016). Landslide investigations in the northwest section of the lesser Khingan range in China using combined HDR and GPR methods. Bull. Eng. Geol. Environ., 75: 591-603. DOI 10.1007/s10064-015-0805-y.

[25] Su, L., Xu, X., Geng, X., & Liang, S. (2016). An integrated geophysical approach for investigating hydro-geological characteristics of a debris landslide in the Wenchuan earthquake area. Engineering Geology. http://dx.doi.org/10.1016/j.enggeo.2016.11.020.

[26] Popescu, M., Şerban, R. D., Urdea, P., & Onaca, A. (2016). Conventional geophysical surveys for landslide investigations: Two case studies from Romania. Carpathian J. Earth and Environ. Sci., 11 (1): 281-292.

[27] Bichler, A., Bobrowsky, P., Best, M., Douma, M., Hunter, J., Calvert, T., & Burns, R. (2004). Three-dimensional mapping of a landslide using a multi-geophysical approach: the Quesnel Forks landslide. Landslides, 1: 29-40. DOI: 10.1007/s10346-003-0008-7.

[28] Otto, J. C., & Sass, O. (2006). Comparing geophysical methods for talus slope investigations in the Turtmann valley (Swiss Alps). Geomorphology, 76: 257-272. doi: 10.1016/j.geomorph.2005.11.008.

[29] Ristić, A., Abolmasov, B., Govedarica, M., & Petrovački, D. (2012). Shallow-landslide spatial Structure interpretation using a multi-geophysical approach. Acta Geotechnica, Slovenica 47-59.

[30] Timothy, R. H., Davies Warburton, J., Stuart A., Dunning Alodie Bubeck, A. P. (2013). A large landslide event in a post-glacial landscape: rethinking glacial legacy. Earth Surface Processes and Landforms, 38 (11): 1261-1268. https://doi.org/10.1002/esp.3377

[31] Lissak, C., Maquaire, O., Malet, J. P., Lavigne Virmoux, C., Gomez, C., & Davidson, R. (2015). Ground-penetrating radar observations for estimating the vertical displacement of rotational landslides. Nat. Hazards Earth Syst. Sci., 15: 1399-1406. doi: 10.5194/nhess-15-1399-2015.

[32] Davis, J. L., & Annan, A. P. (1989). Ground-penetrating radar for high resolution mapping of soil and rock stratigraphy. Geophys. Prosp., 37: 531-551. DOI: 10.1111/j.1365-2478.1989.tb02221.x.

[33] Slater, L., & Niemi, T. M. (2003). Ground penetrating radar investigation of active faults along the Dead Sea transform and implications for seismic hazards within the city of Aqaba, Jordan. Tectonophys, 368: 33-50. DOI: 10.1016/S0040-1951(03)00149-5.

[34] Green, A., Gross, R., Holliger, K., Horstmeyer, H., & Baldwin, J. (2003). Results of 3D georadar surveying and trenching the San Andreas fault near its northern landward limit. Tectonophys, 368: 7-23. doi: 10.1016/S0040-1951(03)00147-1.

[35] Benson, A. K. (1995). Applications of ground penetrating radar in assessing some geological hazards: Examples of groundwater contaminants, faults, cavities. J Appl Geophys 33: 177-193. https://doi.org/10.1016/0926-9851(95)90040-3

[36] Harrari, Z. (1996). Ground penetrating radar (GPR) for imaging stratigraphic features and groundwater in sand dunes, J. Appl. Geophys., 36: 43-52. https://doi.org/10.1016/S0926-9851(96)00031-6

[37] Bano, M., Marquis, G., Niviere, B, Maurin, J. C., & Cushing, M. (2000). Investigating alluvial and tectonic features with ground penetrating radar and analyzing diffractions patterns. J Appl Geophys 43: 3-41. DOI: 10.1016/S0926-9851(99)00031-2.

[38] Bubeck, A., Wilkinson, M., Roberts, G. P., Cowie, P. A., McCaffrey, K. J. W., Phillips, R, & Sammonds, P. (2015). The tectonic geomorphology of bedrock scarps on active normal faults in the Italian Apennines mapped using combined ground penetrating radar and terrestrial laser scanning. Geomorphology, 237: 38-51. DOI: 10.1016/j.geomorph.2014.03.011.

[39] Hatiboğlu, O. (2009). Investigation of Koyulhisar (Sivas) Settlement area in terms of slope instability. Middle East Technical University, MS Thesis, Ankara, Turkey.

[40] UDİM (2016). Uluslararası Deprem İzleme Merkezi (National Earthquake Monitoring Center), Boğaziçi University KOERI (Kandilli Observatory And Earthquake Research Institute). www.koeri.boun.edu.tr/sismo/ (last access: 11.04.2018), Istanbul, Turkey.

[41] MTA (2018). General Directorate of the Mineral Research and Exploration. http://yerbilimleri.mta.gov.tr/anasayfa.aspx (last access: 11.04.2018).

[42] MGM (2016). Turkish State Meteorological Service. Hydrothermal Directorate of Ankara Meteorology Regional Directorate. https://www.mgm.gov.tr/ (accepted: 12.11.2008).

[43] Annan, A. P., Davis, J. L., & Gendzwill, D. (1988). Radar sounding in potash mines: Saskatchewan, Canada. Geophys., 53, 1556-1564.

[44] Wilchek, L. (2000). Ground Penetrating Radar for Detection of Rock Structure. Alberta University, MS Thesis, Canada.

[45] Cardimona, S. (2002). Subsurface investigation using ground penetrating radar. Presented at the 2nd International Conference on the Application of Geophysics and NDT Methodologies Transportation Facilities and Infrastructure, Los Angels, California.

[46] Demirel, Y., & Türk, T. (2022). Investigation of Mass Movements Occurring in Landslide Areas with the Help of Optical Satellite Images: A Case Study in Koyulhisar Town. Photogrammetry Journal of Turkey, 4 (1): 07-16. DOI: 10.53030/tufod.1084630.